Experimental study of the ¹⁶⁵Ho(*n*, 2*n*) reaction: Cross section measurements for the population of the ¹⁶⁴Ho ground state and isomeric state from the threshold up to 20 MeV

E. Georgali ⊙,[1] N. Patronis ⊙,[1] A. Anastasiadis ⊙,[2,3] X. Aslanoglou,[1] M. Axiotis ⊙,[4] Z. Eleme,[1] S. Harissopulos ⊙,[4]
A. Kalamara ⊙,[5] K. Karfopoulos,[6] M. Kokkoris,[5] A. Lagoyannis ⊙,[4] M. Peoviti,[1] C. Potiriadis,[6] M. I. Savva ⊙,[7]
I. E. Stamatelatos,[7] M. E. Stamati ⊙,[1] A. Stamatopoulos ⊙,[5] E. Vagena,[4] T. Vasilopoulou ⊙,[7] and R. Vlastou[5]

¹*Department of Physics, University of Ioannina, 45110 Ioannina, Greece*
²*Department of Physics and Astronomy, Uppsala University, SE-751 05 Uppsala, Sweden*
³*Swedish Radiation Safety Authority, SE-171 16 Stockholm, Sweden*
⁴*Tandem Accelerator Laboratory, Institute of Nuclear and Particle Physics, N.C.S.R. "Demokritos", Aghia Paraskevi, 15310 Athens, Greece*
⁵*Department of Physics, National Technical University of Athens, Zografou Campus, 15780 Athens, Greece*
⁶*Enviromental Radioactivity Monitoring Department, Greek Atomic Energy Commission, 15310 Athens, Greece*
⁷*Institute of Nuclear and Radiological Sciences, Technology, Energy and Safety, N.C.S.R. "Demokritos",
Aghia Paraskevi, 15310 Athens, Greece*

In the present work the ¹⁶⁵Ho(*n*, 2*n*) reaction was studied experimentally and theoretically for the population of the ground state ($J^\pi = 1^+$) of the ¹⁶⁴Ho product nucleus, as well as for the population of its isomeric state ($E_{ex} = 139.8$ keV, $J^\pi = 6^-$). The cross sections of both the ground and isomeric state channels were measured at energies near the reaction threshold ($E_{th} = 8.04$ MeV), at 10.1, 10.4, and 10.7 MeV, as well as at energies higher than 17 MeV, at 17.1, 18.1, 19.0, and 19.6 MeV. The adopted method was the activation technique relative to the ¹⁹⁷Au(*n*, 2*n*)¹⁹⁶Au and ²⁷Al(*n*, *α*)²⁴Na reference reactions. The quasi-monoenergetic neutron beams for the near threshold energies were produced via the ²H(*d*, *n*)³He reaction, while for the neutron beams above 17 MeV the ³H(*d*, *n*)⁴He reaction was utilized. In both cases the deuteron beams were delivered by the 5.5 MV Tandem Van de Graaff accelerator of the Institute of Nuclear and Particle Physics at N.C.S.R. "Demokritos". Additional to the experimental study, calculations were performed using the TALYS code (v. 1.9). The experimental data of the present work along with the previous measurements were compared with the TALYS results so as to investigate the reproduction of the experimental data for the different level density models of the code.

I. INTRODUCTION

The experimental investigation and the improvement of the theoretical modeling of neutron induced reactions is strongly motivated for fundamental research purposes, as well as for applied research purposes, such as the ones that concern energy, medical, and safety applications. Given that a small fraction of the known isotopes is accessible experimentally, the accurate experimental information—when this is feasible—combined with extensive theoretical calculations constitutes a valuable "tool" towards the proper benchmarking and testing of the available broadly used codes. In this way, the theoretical models can be safely validated and later on utilized on unexplored regions of the chart of nuclides.

The neutron induced reactions leading to the formation of different isomers of the residual nuclei are important so as to improve our understanding on the role of nuclear structure in the compound nucleus reaction mechanism. More specifically, the ratio of the cross section of the ground state to the cross section of the isomeric state depends on the spin of these states and the spin distribution of the compound nucleus that populated them. For this reason, the theoretical calculations of these reaction channels can contribute to the investigation of the role of the level density models and their parametrization, as well as to the investigation of the strength of dependency of the excitation function on the spin distribution [1,2]. The ¹⁶⁴Ho nucleus produced by the (*n*, 2*n*) reaction channel of the ¹⁶⁵Ho isotope is formed in the ground state with spin $J^\pi = 1^+$ and in the isomeric state with spin $J^\pi = 6^-$, respectively [3] (see Fig. 1). Consequently, the direct observation of the relative feeding of these states is a sensitive probe of the validity of the level density models of the corresponding theoretical calculations [4]. In addition, it is offered for an investigation about the spin distribution impact on the cross section of both states.

The population of the ground and isomeric state of the ¹⁶⁴Ho isotope as the product-nucleus of the ¹⁶⁵Ho(*n*, 2*n*) reaction channel is depicted in Fig. 1. In the same figure a simplified outline of the decay of these states is also presented, where the states decay mode, half-life, energy levels, and emitted *γ* rays are illustrated [3]. The *γ* rays are presented along with their absolute intensity per 100 decays, which has
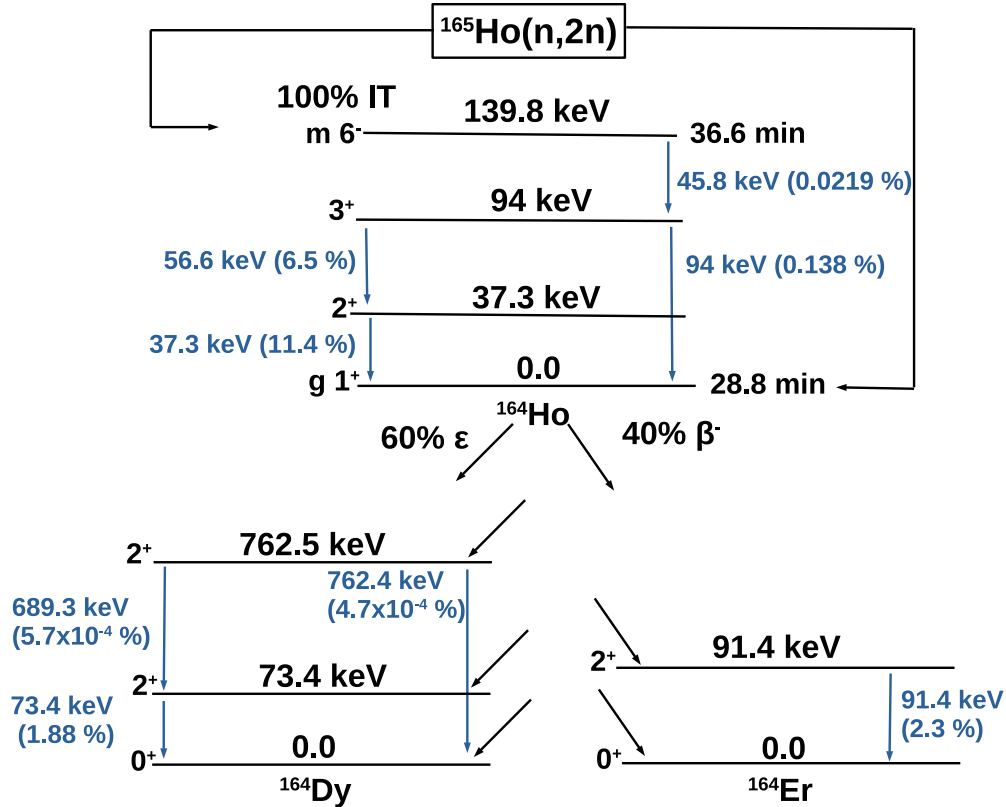
FIG. 1. Simplified representation of the formation and decay of the ground and isomeric state of ^{164}Ho [3].

been calculated considering the competitive decay via internal conversion. As can be seen, ^{164}Ho^m decays to ^{164}Ho^g with 100% isomeric transition (IT). More specifically, the decay follows the IT mode, where the γ emission competes with the internal conversion process [5]. The ^{164}Ho^g isotope decays either to ^{164}Dy via 60% ε or to ^{164}Er via 40% β^-. The decay of the ^{164}Ho^g isotope via the ε process populates any of the energy levels of ^{164}Dy, presented in Fig. 1. Correspondingly, the decay of the ^{164}Ho^g isotope via the β^- process populates either the energy level at 91.4 keV or the ground state of ^{164}Er.

Up to now, several experimental datasets have been reported for both channels. However, no information exists for the excitation functions at energies near the threshold ($E_{th} = 8.04$ MeV), whereas the data for the ground state channel are scarce above 15 MeV. Apart from this, large discrepancies are noticed for the existing data of both channels. For the isomeric state cross section the already existing data are between 12.6–19.5 MeV [6–15], whereas the corresponding range for the ground state is 12.6–18.5 MeV [6,8–11,15,16]. Through the present work the excitation function of the ^{165}Ho($n, 2n$)^{164}Ho^{g+m} reaction was studied in two energy regions: near the reaction threshold and above 17 MeV.

In the following sections the experimental conditions, the data analysis, and the adopted methods of the present study are discussed. Additionally, the cross section results are presented along with the previous data of the literature and they are compared with calculations based on the TALYS (v. 1.9) [17] code.

II. EXPERIMENTAL PROCEDURE

A. Irradiations setup

The ^{165}Ho($n, 2n$) reaction channel cross section was measured via the activation technique in two energy regions: 10.1–10.7 MeV and 17.1–19.6 MeV. The neutron beams were produced through the ^{2}H(d, n)^{3}He ($Q = 3.269$ MeV) and ^{3}H(d, n)^{4}He ($Q = 17.589$ MeV) reactions. In both cases, the deuteron beams were delivered by the 5.5 MV Tandem Van de Graaff accelerator of N.C.S.R. "Demokritos". Each irradiation lasted for 2 h. The neutron beam intensity was determined using the ^{197}Au($n, 2n$)^{196}Au and ^{27}Al(n, α)^{24}Na reference reactions [18].

Four holmium pellets were prepared by mixing 0.55 g of Ho$_2$O$_3$ powder of natural composition (purity $\geqslant$99.99%) with cellulose powder, which was used to improve the mechanical properties of the samples. The Ho$_2$O$_3$ powder was the 90% of the total mass of the pellets. The mixture of Ho$_2$O$_3$ and cellulose was pressed so that the pellets would have 1 mm thickness and 13 mm diameter. During the irradiations, each holmium sample was "sandwiched" between Au and Al monitor foils of equal diameter.

In the case of the low energy neutron beams, between 10.1–10.7 MeV, deuteron beams of 1.5 μA were directed to a D_2 gas target. During the irradiations, the gas target was cooled via a cold air jet to minimize the effect of heating in the deuterium gas. The pressure was kept constant at 1250 mbar via a micrometric valve. The entrance window of the gas target consisted of a Mo foil with 5 μm thickness, whereas
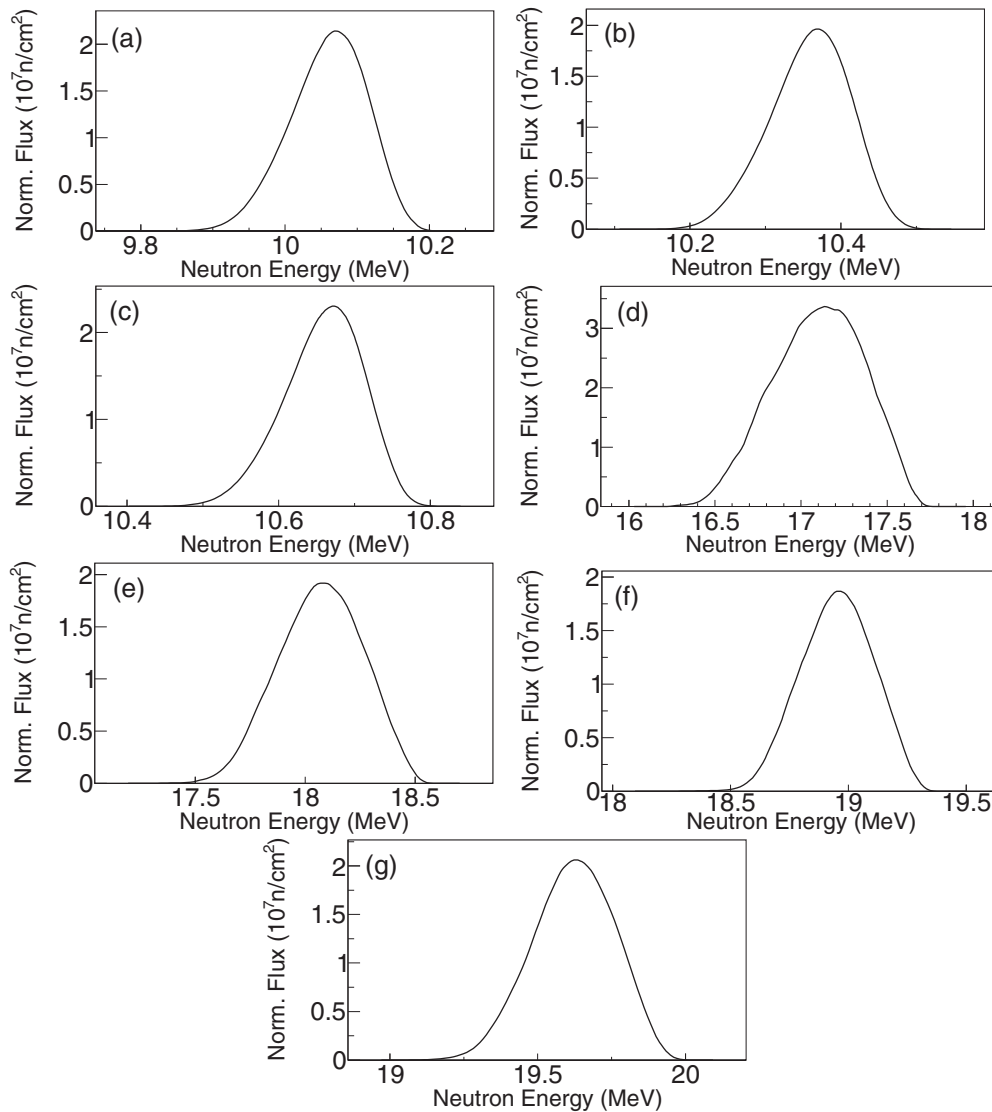
FIG. 2. Neutron energy spectra as resulted from the NEUSDESC code [19] for each irradiation: (a) 10.1 ± 0.1 MeV, (b) 10.4 ± 0.1 MeV, (c) 10.7 ± 0.1 MeV, (d) 17.1 ± 0.3 MeV, (e) 18.1 ± 0.2 MeV, (f) 19.0 ± 0.2 MeV, (g) 19.6 ± 0.2 MeV. The spectra are normalized to the total neutron flux (n/cm^2), as calculated from the reference foils.

a Pt foil was used as the beam stop of the gas cell. The samples were irradiated at 0° with respect to the primary deuteron beam and at 7 cm distance from the center of the gas cell. The neutron flux for all irradiations varied between 7.8×10^4–9.5×10^4 n/(cm^2 s).

On the other hand, for the high energy neutron beams, between 17.1–19.6 MeV, deuteron beams of 300 nA were impinging on a 2.1 mg/cm^2 Ti-tritiated target, which was supported by an 1 mm thick Cu backing for optimum heat conduction purposes. Two Mo foils of 5 μm in thickness each served as entrance foils in the target to decelerate the deuteron beam. The deuteron beam energy should be higher than 2.5 MeV, where the transmission of the accelerator is optimum. The target configuration was air cooled during the irradiations to avoid possible temperature increase. The samples were placed at 0° with respect to the primary deuteron beam, as in the case of the low energy irradiations, but a shorter primary target-samples distance was adopted, namely

2.5 cm with respect to the center of the Ti-tritiated target. The neutron flux for all irradiations varied between 8.3×10^4–1.8×10^5 n/(cm^2 s).

For the calculation of the neutron beams energy distribution, the NEUSDESC code [19] was used. NEUSDESC calculates the energy loss, as well as the angular and energy straggling of the deuteron beam in the structural materials of the D_2 gas and the Ti-tritiated targets by its interplay with SRIM-2008 Monte Carlo simulation program [20]. The neutron energy distribution normalized to the total neutron flux (n/cm^2), as calculated from the reference foils, is presented in Fig. 2 for each irradiation. Calculations were also performed through the GEANT4 Monte Carlo simulation code [21], where the deuteron beam transportation was modeled along with the DD and DT reactions. The deuteron beam optics elements, as well as all the structural materials of the beam line were taken into account. The results were consistent with the corresponding results of NEUSDESC. Furthermore, calculations of the neutron
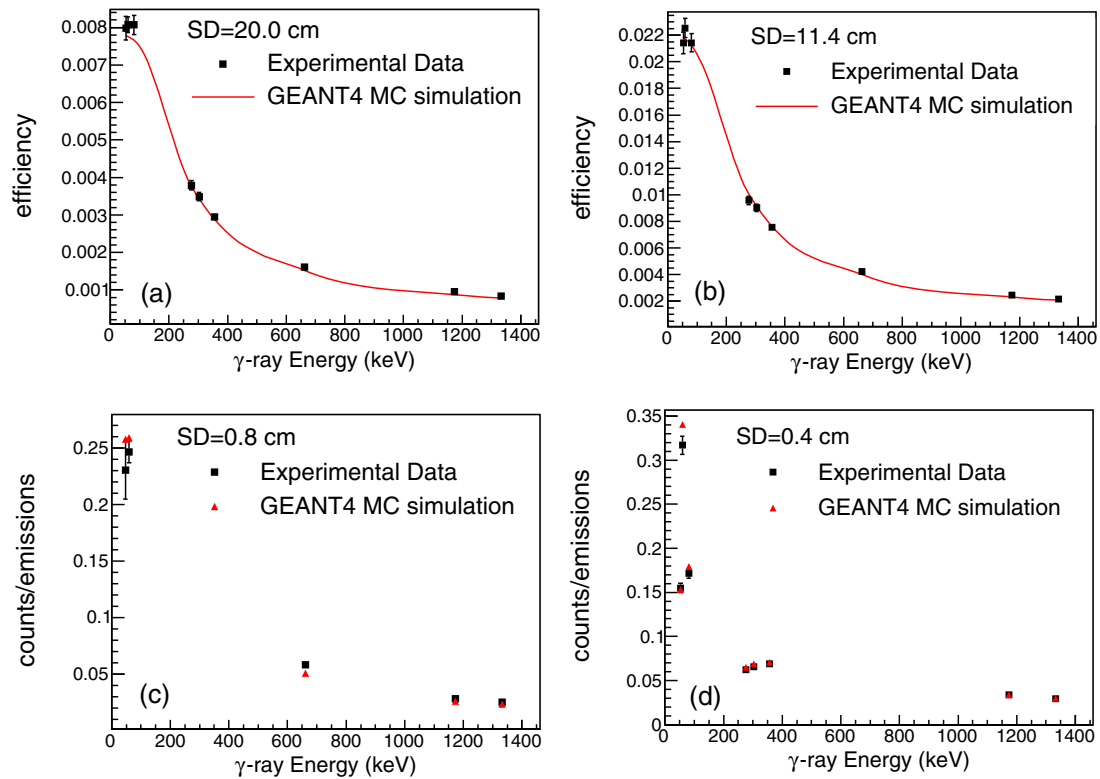
FIG. 3. Comparison of the experimental efficiency and counting rate data of the 50% relative efficiency broad energy HPGe detector with the GEANT4 MC code simulations at the distances of (a) 20 cm, (b) 11.4 cm, (c) 0.8 cm, and (d) 0.4 cm. In (a) and (b) the efficiency of the detector is presented for the distances of 20 and 11.4 cm. In (c) and (d) the ratio of the recorded photopeak counts to the corresponding emissions is presented for the distances of 0.8 and 0.4 cm. As can be seen, by including the full decay schemes in the GEANT4 simulations, the observed counts/emissions ratios were successfully reproduced.

beams energy distribution had also been performed in the past with other simulation codes such as MCNP5 [22,23].

The deuteron beam current in the primary targets was recorded by means of a multichannel scaler and an analog-to-digital converter every 10 s. Moreover, the neutron beam was monitored by a BF_3 counter, placed at the distance of 3 m and in 20° with respect to the deuteron beam direction. In this way, the neutron counting rate was also recorded every 10 s. The deuteron and neutron beam fluctuations were used to accurately calculate the factors correcting for the product-nuclei decay during irradiations (presented in Sec. III).

B. Activity measurements

After the end of each irradiation, the measurements of the induced activity of the holmium targets and the reference foils were performed.

For the holmium targets a broad energy HPGe coaxial detector was used with 50% relative efficiency. Its window consisted of carbon fibres and the front-contact crystal dead layer was a few μm thick. Both these features lead to minimization of the attenuation of the low energy γ rays, allowing the efficient detection even if their energy is a few keV.

The usage of a broad energy detector for the ^{164}Ho activity measurements was a prerequisite, given that the γ rays emitted are located between 37.3–91.4 keV [3]. The holmium targets were placed at 1.5 mm distance from the detector window. The close measurement geometry was chosen so as to maximize the counting rate. The latter was necessary given 1) the low intensity of some γ rays [3] and 2) the strong self-attenuation of the low energy γ rays.

For the accurate determination of the full-energy peak efficiency of the HPGe detector at the actual detection geometry, the GEANT4 Monte Carlo simulation code was extensively used. The simulations were compared and validated with experimental efficiency and counting rate data towards a comprehensive characterization of the detector. At close detection geometries, the decay schemes of the isotopes were taken into consideration in order to reproduce possible coincidence summing effects. For the simulations of the long source-to-detector distances, the γ rays were emitted monoenergetically considering that at these distances the coincidence summing effects are negligible. In Fig. 3 the experimental efficiency and counting rate data are presented along with the corresponding results of the GEANT4 simulations.

For the reference foils activity measurements, an 80% relative efficiency HPGe detector was used. The foils were placed at a distance of 1 cm from the detector window. Such a close detection geometry was chosen to compensate for the short irradiations comparing with the half-lives of the reference foils product nuclei [24,25].

As previously, by adopting such a close detection geometry special care had to be taken for the consideration of the correction factor related to coincidence summing effects.
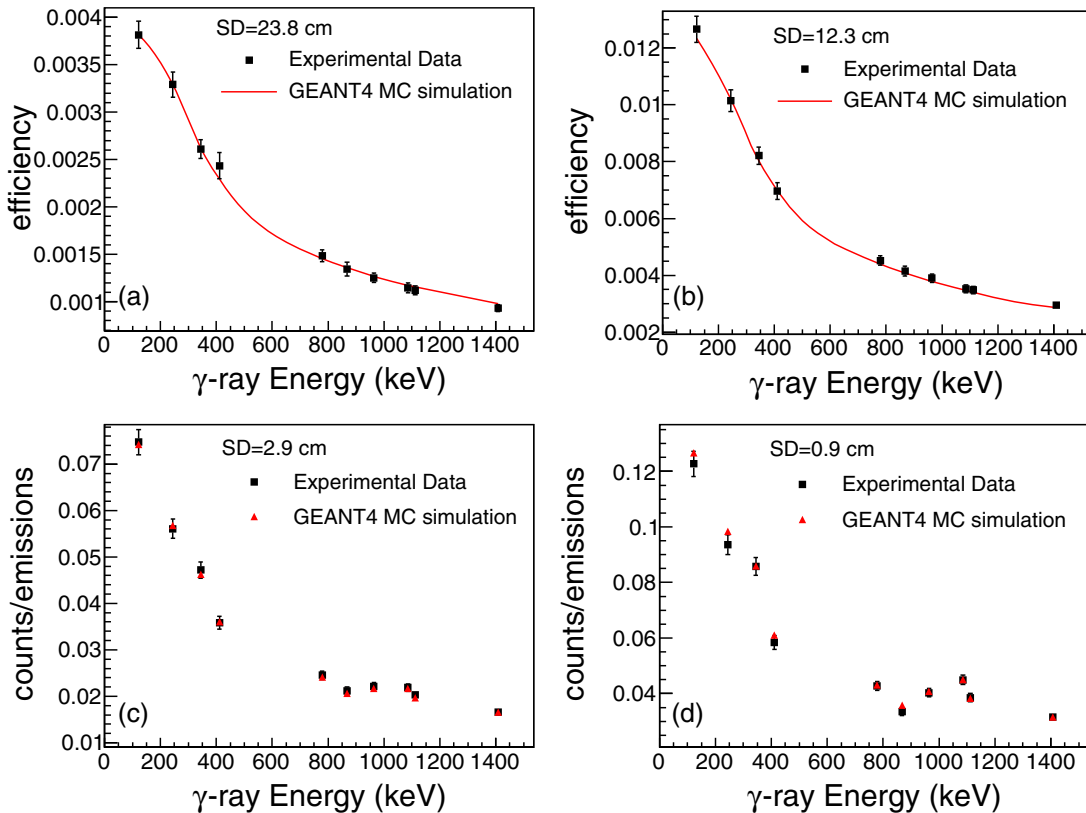
FIG. 4. Comparison of the experimental efficiency and counting rate data of the 80% relative efficiency HPGe detector with the GEANT4 MC code simulations at the distances of (a) 23.8 cm, (b) 12.3 cm, (c) 2.9 cm, and (d) 0.9 cm. In (a) and (b) the efficiency of the detector is presented for the distances of 23.8 and 12.3 cm. In (c) and (d) the ratio of the recorded photopeak counts to the corresponding emissions is presented for the distances of 2.9 and 0.9 cm. As can be seen, by including the full decay scheme of ^{152}Eu in the GEANT4 simulations, the observed counts/emissions ratios were successfully reproduced.

For this reason, a ^{152}Eu [26] point source was used and the crystal dimensions of the 80% HPGe detector were adjusted in the GEANT4 simulations so as to reproduce experimental efficiency and counting rate data for the given activity of the source and for several source-to-detector distances (23.8 cm, 12.3 cm, 2.9 cm, and 0.9 cm). At long distances the inclusion of the decay scheme was not important, but at short distances the consideration of the decay scheme was crucial for the interpretation of the observed full-energy peak counting rate of each decay line. The results of this validation process are presented in Fig. 4.

III. DATA ANALYSIS

A. Activation technique

In the analysis of the experimental data both of the aforementioned stages of activation technique were considered. In this way, by combining the equations providing the number of activated nuclei at the end of the irradiation and the measured induced activity of the samples, the corresponding cross section value can be determined. Under this scope, the number of activated nuclei in the isomeric state at the end of the irradiation N_0^m is given by Eq. (1):

$$N_0^m = \sigma_m \Phi N_T f_B, \tag{1}$$

where Φ is the time integrated neutron flux, σ_m is the ^{165}Ho(n, 2n) ^{164}Ho^m reaction cross section, and N_T is the number of ^{165}Ho nuclei in the target. f_B is the correction factor for the decay during the irradiation time (t_{ir}) of the N_{act}^m activated in the isomeric state nuclei:

$$f_B = \frac{\int_0^{t_{ir}} \mathrm{flux}(t) e^{\lambda_m t} dt}{\int_0^{t_{ir}} \mathrm{flux}(t) dt} e^{-\lambda_m t_{ir}}, \tag{2}$$

where λ_m is the decay constant of the isomeric state.

The induced activity A_m, as measured from the γ rays resulting from the N_{act}^m decay to the ground state of ^{164}Ho is equal to

$$A_m = \frac{I_m \varepsilon_m N_0^m e^{-\lambda_m t_w} (1 - e^{-\lambda_m t_m})}{C_{DT}}. \tag{3}$$

The factor C_{DT} corresponds to dead-time corrections, whereas the factor I_m is the intensity of the γ ray. The term ε_m corresponds to the efficiency of the HPGe detector for the γ-ray energy at the geometry of the measurement, including the self-attenuation and coincidence summing effects corrections. The t_m and t_w terms stand for the activity measurement time and the time interval between the end of the irradiation and the start of the measurement, "waiting time", respectively.

TABLE I. Decay properties of the product-nuclei.

Product nucleus	Half-life	γ-ray energy (keV)	Intensity per decay (%)
^{164}Ho^m [3]	(36.6 ± 0.3) min	37.3	11.4 ± 0.7
^{164}Ho^g [3]	(28.8 ± 0.5) min	73.4	1.88 ± 0.21
		91.4	2.3 ± 0.3
^{196}Au [24]	(6.1669 ± 0.0006) d	355.7	87
^{24}Na [25]	(14.997 ± 0.012) h	1368.6	99.9936 ± 0.0015

By combining Eqs. (1) and (3) the cross section of the ^{165}Ho$(n, 2n)$ ^{164}Ho^m reaction can be calculated:

$$\sigma_m = \frac{A_m C_{DT}}{\Phi N_T \varepsilon_m I_m e^{-\lambda_m t_w}(1 - e^{-\lambda_m t_m})f_B}. \quad (4)$$

The case of the ^{165}Ho$(n, 2n)$ ^{164}Ho^g reaction channel is more complicated. Due to fact that the ground and the isomeric state of ^{164}Ho have similar half-lives ($T_{1/2}^m = 36.6$ and $T_{1/2}^g = 28.8$ min, respectively [3]), the ground state population coming from the isomeric state must be considered during the irradiation, the "waiting" and the activity measurement times. For this reason, the number of nuclei in the ground state at the end of the irradiation, N_0^g, is equal to

$$N_0^g = \sigma_g \Phi N_T f_B' + \sigma_m \Phi N_T f_C. \quad (5)$$

The term σ_g is the ^{165}Ho$(n, 2n)$ ^{164}Ho^g reaction cross section. The $\sigma_g \Phi N_T f_B'$ quantity corresponds to the number of activated nuclei in the ground state produced directly from the ^{165}Ho$(n, 2n)$ ^{164}Ho^g reaction channel. On the other hand, the $\sigma_m \Phi N_T f_C$ term is equal to the number of activated nuclei in the ground state produced from the ^{164}Ho^m decay. The correction factors f_B' and f_C refer to the decay of the ground state (N_{act}^g) during the irradiation time and are calculated according to the Eqs. (6) and (7):

$$f_B' = \frac{\int_0^{t_{ir}} \text{flux}(t)e^{\lambda_g t} dt}{\int_0^{t_{ir}} \text{flux}(t) dt} e^{-\lambda_g t_{ir}}, \quad (6)$$

$$f_C = \frac{\int_0^{t_{ir}} \text{flux}(t)e^{\lambda_g t} dt}{\int_0^{t_{ir}} \text{flux}(t) dt} e^{-\lambda_g t_{ir}} - \frac{\int_0^{t_{ir}} \text{flux}(t)e^{(\lambda_g - \lambda_m)t} dt}{\int_0^{t_{ir}} \text{flux}(t) dt} e^{-\lambda_g t_{ir}}, \quad (7)$$

where λ_g is the decay constant of the ground state.

The corresponding activity, as measured from the γ rays emitted from the ^{164}Ho^g activated nuclei, is concluded to be equal to

$$A_g = \varepsilon_g I_g \left(\frac{N_0^g D_g}{C_{DT}} + \frac{N_0^m \frac{1}{\lambda_g - \lambda_m}(\lambda_g D_m - \lambda_m D_g)}{C_{DT}} \right). \quad (8)$$

As mentioned previously, I_g is the intensity of the γ ray coming from the decay of the ground state and ε_g is the detector efficiency for this γ ray, where self-attenuation and coincidence summing effects have been taken into account. The terms D_g and D_m are equal to $D_g = e^{-\lambda_g t_w}(1 - e^{-\lambda_g t_m})$ and $D_m = e^{-\lambda_m t_w}(1 - e^{-\lambda_m t_m})$. They originate from the

consideration of the ground and isomeric state decay during the measurement and the "waiting time".

Finally, the ^{165}Ho$(n, 2n)$ ^{164}Ho^g reaction cross section σ_g is calculated through the combination of Eqs. (5) and (8):

$$\sigma_g = \frac{A_g C_{DT}}{\Phi N_T \varepsilon_g I_g D_g f_B'} - \sigma_m \left(\frac{f_B}{f_B'} \frac{\frac{1}{\lambda_g - \lambda_m}(\lambda_g D_m - \lambda_m D_g)}{D_g} + \frac{f_C}{f_B'} \right). \quad (9)$$

It has to be noted that the first term of Eq. (9) is the same with the standard equation of activation technique for the calculation of the cross section when the feeding from an isomeric state is absent or can be ignored [4] [see also Eq. (4)]. The second term describes the contribution from the isomeric state and must be subtracted from the first one so as to correct for the isomeric state decay to the ground state of ^{164}Ho.

The dead-time correction factor C_{DT} was calculated as the ratio of the "real-time" of the measurement to the "live-time" for which the data acquisition system was active. However, its value was found to be negligible: less than 0.02%. As mentioned previously, the self-attenuation corrections were incorporated in the efficiency calculations. This was achieved by defining in the GEANT4 simulations the suitable target material. The targets thickness uncertainty, however, affects the total efficiency uncertainty, since thicker or thinner targets cause higher or lower self-attenuation. The targets thickness uncertainty was 2%. This uncertainty was included in the given total efficiency uncertainty (5%). Furthermore, a sensitivity test was performed by changing the thickness of the targets for a value of ± 0.05 mm. The test revealed that even for such an extreme change in the targets thickness, the results agree with the efficiency values for the actual targets thickness (1 mm) within 5%. Concerning the coincidence summing effect, the corrections were again incorporated in the efficiency calculations by considering in the simulations the full decay schemes of the ^{164}Ho^g and ^{164}Ho^m isotopes.

As mentioned previously, the neutron flux Φ was deduced using reference foils of Au and Al, placed on both sides of the holmium targets. Specifically, the time integrated neutron flux was obtained solving the aforementioned equations with respect to Φ. The ^{197}Au$(n, 2n)$ ^{196}Au and ^{27}Al(n, α) ^{24}Na reference reactions cross section were taken from Ref. [18].

The decay data of the product-nuclei of the holmium targets [3] and the reference foils [24,25] are presented in Table I. The irradiation time, the measuring time, the time integrated flux and the f_B, f_B', and f_C correction factors for each irradiation are summarized in Table II.

TABLE II. Summary of the irradiation and measurement parameters.

	10.1 MeV	10.4 MeV	10.7 MeV
Irradiation time (min)	125	126	118
Time integrated flux ($\times 10^8$ n/cm^2)	6.33 ± 0.44	6.02 ± 0.42	6.92 ± 0.48
Decay correction factor f_B for the holmium target	0.3879	0.3921	0.4078
Decay correction factor f_B' for the holmium target	0.3206	0.3266	0.3400
Decay correction factor f_C for the holmium target	0.2510	0.2591	0.2595
Measuring time (min)	110	90	93

	17.1 MeV	18.1 MeV	19.0 MeV	19.6 MeV
Irradiation time (min)	121	120	121	119
Time integrated flux ($\times 10^8$ n/cm^2)	12.65 ± 0.88	6.45 ± 0.45	5.36 ± 0.38	6.67 ± 0.47
Decay correction factor f_B for the holmium target	0.3929	0.3947	0.3891	0.3919
Decay correction factor f_B' for the holmium target	0.3255	0.3270	0.3227	0.3243
Decay correction factor f_C for the holmium target	0.2508	0.2459	0.2473	0.2461
Measuring time (min)	125	105	120	90

B. Isomeric state decay line at 37.3 keV

The ^{164}Ho nucleus, produced by the $(n, 2n)$ channel of the ^{165}Ho isotope, emits during its decay γ rays in the energy range: 37.3 keV–91.4 keV [3]. In this energy region the peak-analysis procedure is a complicated process due to the expected x rays coming from the holmium activated target, as well as due to the x-ray escape peaks which are also present at low energies.

X-ray escape peaks arise when a portion of x rays, with energy above the Ge K-edge $= 11.1$ keV, are absorbed by the Ge volume. The energy absorbed can be recombined with the initial energy after the Ge de-excitation or it can escape from the detector active volume if the interaction occurs near the crystal edge. In this case, x-ray escape peaks are detected at 9.8 keV and 11.0 keV lower energies. The latter values are the average energies of the K_α and K_β x-ray emission lines of Ge [27].

In the ^{164}Ho decay spectrum x-ray peaks appear at energies between 45.2–57.1 keV. Six of them are emitted between 45.2–49.1 keV [3]. As a result, escape peaks arise at 37.3 keV and in the neighboring region. The photopeak at 37.3 keV is the one used for the ^{165}Ho$(n, 2n)$ ^{164}Ho^m reaction cross section determination.

To deal with this feature, the GEANT4 simulation toolkit was utilized once more. After having fully characterized the broad energy HPGe detector, as described in Sec. II, the reproduction of the ^{164}Ho decay spectrum was achieved. This was necessary in order to resolve the counts within the 37.3 keV photopeak attributed to the γ-decay line of the isomeric state against the x-ray escape peaks. The experimental counts at 37.3 keV photopeak were calculated by multiplying the experimental counts between 34.5–39 keV with the ratio of the simulation counts at 37.3 keV (A) to the simulation counts between 34.5–39 keV (B). Under this scope, the uncertainty in the counting statistics at 37.3 keV is coming i) from the counting statistics at 34.5–39 keV energy region and ii) from the A/B ratio. To evaluate the uncertainty of this ratio, the experimental spectra were reproduced for slightly different number of emissions for the decays of the ^{164}Ho ground and

isomeric state. The number of emissions was checked so as to reproduce the counts of the 91.4 and 73.4 keV photopeaks (coming from ^{164}Ho^g), as well as the 84 and 84.9 keV photopeaks (coming from the coincidence summing of the 37.3 keV γ ray with the x rays at 46.7 and 47.5 keV, which are emitted by ^{164}Ho^m). All tests of reproduction of the spectra with different number of emissions led to the same value for the A/B ratio for each spectrum. Therefore, the uncertainty that was adopted in the analysis is the uncertainty of the experimental counting statistics between 34.5–39 keV.

Figure 5 depicts the background subtracted experimental spectrum of the ^{164}Ho decay for the neutron beam energy of 10.1 MeV and after 92 min of data acquisition time along with the respective simulation. The contribution of the room background to the experimental spectrum was almost negligible due to the crystal geometry, the short duration of the measurement and the carefully designed shielding of the detector. Despite this, in Fig. 5 the background subtracted spectrum is presented for a direct comparison with the GEANT4 Monte Carlo simulation. The impact of the background subtraction in the overall statistical uncertainty was also found negligible.
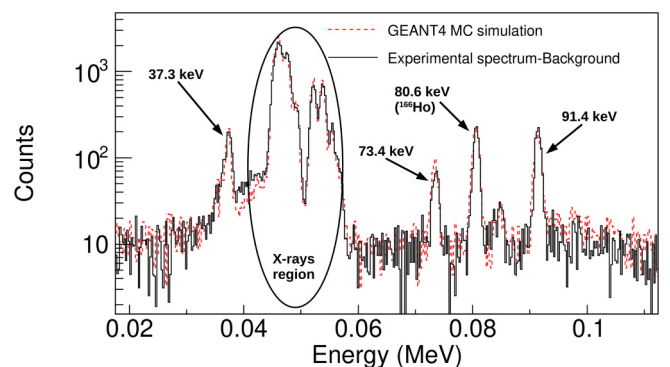

FIG. 5. The background subtracted ^{164}Ho experimental spectrum for $E_n = 10.1$ MeV and 92 min of measurement. In the same figure the respective GEANT4 simulation is illustrated.

TABLE III. Measured cross section values for the ^{165}Ho$(n, 2n)^{164}$Ho^m and ^{165}Ho$(n, 2n)^{164}$Ho^g reaction channels.

E_n (MeV)	σ_m (mb)	σ_g (mb)
10.1 ± 0.1	324 ± 42	434 ± 104
10.4 ± 0.1	327 ± 43	529 ± 106
10.7 ± 0.1	390 ± 48	661 ± 114
17.1 ± 0.3	640 ± 71	642 ± 148
18.1 ± 0.2	592 ± 67	576 ± 139
19.0 ± 0.2	492 ± 58	490 ± 131
19.6 ± 0.2	387 ± 46	318 ± 90

IV. EXPERIMENTAL RESULTS

Implementing the activation technique the cross sections of the ^{165}Ho$(n, 2n)^{164}$Ho^m and ^{165}Ho$(n, 2n)^{164}$Ho^g reactions were measured near threshold energies ($E_{th} = 8.04$ MeV), at 10.1, 10.4, and 10.7 MeV, as well as at 17.1, 18.1, 19.0, and 19.6 MeV. For both reactions the previous measurements of the cross sections are discrepant and they all refer to energies above 12.5 MeV [28]. Through the present work the mapping of the excitation functions of the ^{165}Ho$(n, 2n)^{164}$Ho^m and ^{165}Ho$(n, 2n)^{164}$Ho^g reactions could be significantly improved.

The present results are depicted in Table III. As mentioned, the cross section of the isomeric state was deduced by the analysis of the photopeak at 37.3 keV. The cross section of the ground state was calculated as the weighted average of the cross sections deduced using the photopeaks at 73.4 keV and 91.4 keV:

$$\langle \sigma \rangle = \frac{(V_2 - V_{12})\sigma_1 + (V_1 - V_{12})\sigma_2}{V_1 + V_2 - 2V_{12}}, \qquad (10)$$

$$\mathrm{var}(\sigma) = \frac{V_1 V_2 - (V_{12})^2}{V_1 + V_2 - 2V_{12}}. \qquad (11)$$

In the above equations σ_1 and σ_2 stand for the individual cross sections, resulting from the analysis of the 73.4 keV and 91.4 keV photopeaks. V_1 and V_2 are the respective variances of the cross sections, which are equal to the square of the uncertainties. Finally, V_{12} is the covariance element between σ_1 and σ_2 and it is given by Eq. (12):

$$V_{12} = \frac{\partial \sigma_1}{\partial \Phi_1} \mathrm{Cov}(\Phi_1, \Phi_2) \frac{\partial \sigma_2}{\partial \Phi_2} + \frac{\partial \sigma_1}{\partial N_{T1}} \mathrm{Cov}(N_{T1}, N_{T2}) \frac{\partial \sigma_2}{\partial N_{T2}}$$
$$+ \frac{\partial \sigma_1}{\partial \mathrm{Counts}_1} \mathrm{Cov}(\mathrm{Counts}_1, \mathrm{Counts}_2) \frac{\partial \sigma_2}{\partial \mathrm{Counts}_2}$$
$$+ \frac{\partial \sigma_1}{\partial \varepsilon_{m1}} \mathrm{Cov}(\varepsilon_{m1}, \varepsilon_{m2}) \frac{\partial \sigma_2}{\partial \varepsilon_{m2}} + \frac{\partial \sigma_1}{\partial I_{m1}} \mathrm{Cov}(I_{m1}, I_{m2}) \frac{\partial \sigma_2}{\partial I_{m2}}, \qquad (12)$$

In our case, the above correlations emanate from the following facts: 1) the time integrated neutron flux was the same: $\Phi_1 = \Phi_2 = \Phi$, 2) the number of the ^{165}Ho nuclei in the target was the same, since one sample was used for each irradiation: $N_{T1} = N_{T2} = N_T$, 3) the same photopeak at 37.3 keV was used to correct for the isomeric state population: Counts$_1$ = Counts$_2$ = Counts, $\varepsilon_{m1} = \varepsilon_{m2} = \varepsilon_m$, and $I_{m1} = I_{m2} = I_m$.

In Table IV the uncertainties contributing to the total uncertainty of the measured cross sections are given.

V. TALYS CALCULATIONS

The cross section measurements of the present study, as well as the previous ones were compared with calculations performed using the TALYS code.

TALYS calculates the cross section for all the possible channels of the interaction under study and as a result, the competition between all channels is considered. The compound nucleus interactions are taken into account in the Hauser-Feshbach theory [29], whereas for the pre-equilibrium mechanism the default option based on exciton model calculations, as described in Refs. [30–32], was adopted. For the direct reaction calculations the default option and the one used is the coupled-channels model [33].

Calculations were performed for all the phenomenological level density models provided by the code: constant temperature model [34], back-shifted Fermi gas model [35], and generalized superfluid model [36,37]. Calculations were also performed for the microscopic level density models: Coriely *et al.* [38] (microscopic model 1), Goriely *et al.* [39] (microscopic model 2), and Hilaire *et al.* [40] (microscopic model 3). The adoption of different level density models revealed different behaviors in the excitation function of the ^{165}Ho$(n, 2n)^{164}$Ho^m and ^{165}Ho$(n, 2n)^{164}$Ho^g reactions. In order to investigate the sensitivity of the reactions cross section on the optical potential and γ-ray strength function models, more calculations were performed using fixed level density models. Initially, it was investigated if the two optical models of Koning-Delaroche [41] and Bauge *et al.* [42], which are provided by the code for neutron incident particles, produce compatible results. The outcome revealed that the cross section of the reactions under study is independent on the selection of the optical potential.

Concerning the γ-ray strength function models, TALYS uses a fixed γ-ray strength function model, the Brink-Axel Lorentzian one [43,44], for all the transitions, apart from the $E1$. For the $E1$ transition two phenomenological models are incorporated, the Kopecky-Uhl generalized Lorentzian model [45], as well as the Brink-Axel Lorentzian model [43,44]. Furthermore, six microscopic models are available [17,46]. All models provided similar results, when the Back-Shifted Fermi Gas model [35] and the three microscopic ones [38–40] were used for the level density calculations. A stronger dependency on the selection of the γ-ray strength function model for the $E1$ transition was noticed for the constant temperature [34] and the generalized superfluid [36,37] models. In these calculations some microscopic γ-ray strength function models (models: 3, 4, and 8 of TALYS) presented larger discrepancies from the data at near threshold energies than the rest models, which produced compatible results. In addition, in the case of the generalized superfluid model [36,37] a slightly better agreement with the data of the present work for the isomeric state channel resulted for the Kopecky-Uhl generalized Lorentzian model [45].

As reported in the literature (e.g., Ref. [1]), the relative feeding of the isomeric and ground state can be used as a

TABLE IV. Compilation of uncertainties (in %).

E_n (MeV)	10.1	10.4	10.7	
reference reaction		^{197}Au$(n, 2n)$ ^{196}Au		
reference reaction cross section	3.0	3.0	2.8	
neutron flux	7.0	7.0	7.0	
37.3 keV peak counting statistics	7.1	7.6	6.3	
73.4 keV peak counting statistics	6.8	7.0	5.3	
91.4 keV peak counting statistics	3.7	3.7	3.0	
BE5030 HPGe detector efficiency	5.0	5.0	5.0	
37.3 keV γ-ray intensity per decay	6.3	6.3	6.3	
targets thickness	2.0	2.0	2.0	
reference foils peak counting statistics (front-back)	2.5–2.7	1.2–1.6	1.6–2.2	
80% HPGe detector efficiency	3.0	3.0	3.0	
reference foils γ-ray intensity per decay	–	–	–	
statistical uncertainty of cross section for isomeric state	7.1	7.6	6.3	
systematic uncertainty of cross section for isomeric state	10.7	10.7	10.7	
total uncertainty of cross section for isomeric state	13	13	12	
statistical uncertainty of cross section for ground state	15.2	12.7	9.5	
systematic uncertainty of cross section for ground state	17.7	14.7	13.9	
total uncertainty of cross section for ground state	24	20	17	
E_n (MeV)	17.1	18.1	19.0	19.6
reference reaction		^{24}Al(n, α) ^{24}Na		
reference reaction cross section	0.83	0.98	1.19	1.31
neutron flux	7.0	7.0	7.0	7.0
37.3 keV peak counting statistics	2.9	4.2	5.2	5.4
73.4 keV peak counting statistics	2.9	4.5	5.8	6.2
91.4 keV peak counting statistics	1.8	2.9	3.7	3.7
BE5030 HPGe detector efficiency	5.0	5.0	5.0	5.0
37.3 keV γ-ray intensity per decay	6.3	6.3	6.3	6.3
targets thickness	2.0	2.0	2.0	2.0
reference foils peak counting statistics (front-back)	0.5–1.5	2.5–2.8	3.0–4.0	3.4–3.9
80% HPGe detector efficiency	3.0	3.0	3.0	3.0
reference foils γ-ray intensity per decay	0.0015	0.0015	0.0015	0.0015
statistical uncertainty of cross section for isomeric state	2.9	4.0	5.2	5.4
systematic uncertainty of cross section for isomeric state	10.7	10.7	10.7	10.7
total uncertainty of cross section for isomeric state	11	11	12	12
statistical uncertainty of cross section for ground state	7.9	11.3	15.1	16.3
systematic uncertainty of cross section for ground state	21.5	21.2	22	22.3
total uncertainty of cross section for ground state	23	24	27	28

"probe" for the study of the spin distribution of the populated excited states of the compound nucleus. For this reason, as an additional stage of the validation procedure of the calculations, the "Rspincut" TALYS keyword was modified (default value=1). Specifically, this keyword is a multiplication factor of the spin cut-off parameter σ_F^2. The latter stands for the width of the angular momentum distribution and is given by Eq. (13):

$$\sigma_F^2 = 0.01389 \frac{A^{\frac{5}{4}}}{\hat{\alpha}} \sqrt{\alpha U}, \qquad (13)$$

where A is the mass number, U is the effective excitation energy defined as $U = E_x - \Delta$ (E_x is the true excitation energy and Δ is equal to, or for some models closely related to, the pairing energy which simulates odd-even effects). The parameter α is the energy dependent level density parameter, which takes into account the existence of shell effects at low energies and the damping of the latter as the excitation energy increases, according to Eq. (14):

$$\alpha = \alpha(E_x) = \hat{\alpha}\left(1 + \delta W \frac{1 - \exp^{-\gamma U}}{U}\right). \qquad (14)$$

The terms δW and γ stand for the shell correction energy and the damping parameter of shell effects with increasing excitation energy, respectively. The parameter $\hat{\alpha}$ is called asymptotic level density parameter and is equal to α when shell effects are absent.

In the above calculations the full j, l coupling was considered in the Hauser-Feshbach theory (TALYS keyword: "fullhf").

The TALYS calculations corresponding to the cross section of the isomeric state along with the experimental data of the present and previous studies are presented in Fig. 6, while in
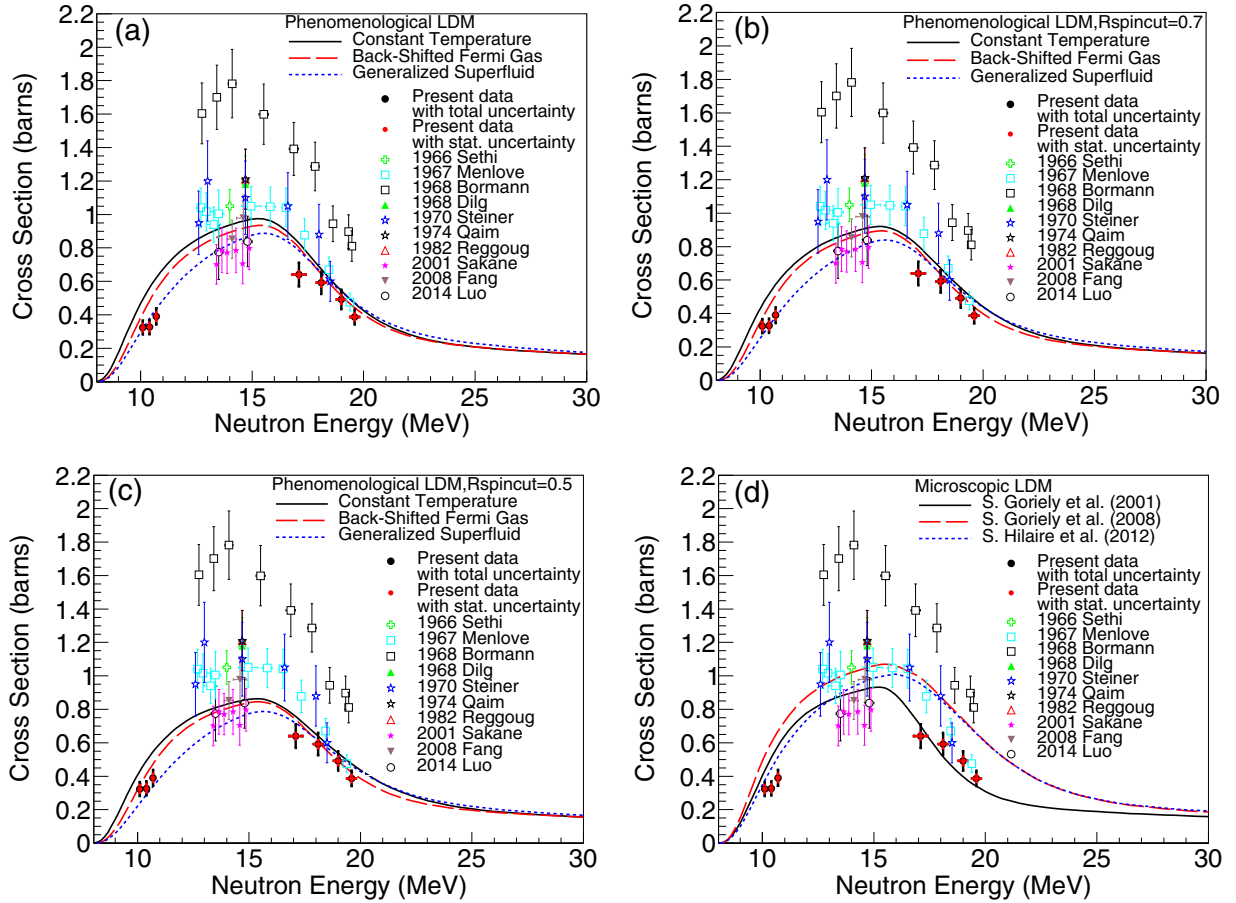
FIG. 6. The experimental data of the present study and previous studies for the ^{165}Ho$(n, 2n)$ ^{164}Ho^m reaction along with the calculations based on the TALYS code (v. 1.9) for (a) the three phenomenological level density models: constant temperature model [34], back-shifted Fermi gas model [35], generalized superfluid model [36,37], (b) the three phenomenological level density models after setting "Rspincut" keyword equal to 0.7, (c) the three phenomenological level density models after setting "Rspincut" keyword equal to 0.5, and (d) the three microscopic level density models: Coriely *et al.* [38] (microscopic model 1), Goriely *et al.* [39] (microscopic model 2), and Hilaire *et al.* [40] (microscopic model 3). The experimental cross section data of the present work are presented with two different error bars corresponding to the statistical and total uncertainties.

Fig. 7 the respective results for the ground state channel can be seen. In both Figs. 6 and 7 two different error bars are shown. They correspond to the statistical and to the total (sum of the statistical and systematic) uncertainties. In Fig. 8 the ratio of the ground to the isomeric state cross section is given. The models and the parametrization used in these calculations are summarized in Table V.

VI. RESULTS AND DISCUSSION

Through the present work the cross sections of the ^{165}Ho$(n, 2n)$ ^{164}Ho^m and ^{165}Ho$(n, 2n)$ ^{164}Ho^g reaction channels have been measured at 10.1, 10.4, 10.7, 17.1, 18.1, 19.0, and 19.6 MeV neutron beam energies via the activation technique. Using the TALYS code (v. 1.9), cross section calculations have also been performed so as to compare the experimental data with theoretical estimations. A first test was executed searching the calculations performance for all the level density models of the code (Figs. 6–8). More tests were performed searching the impact of different optical potentials (Koning-Delaroche [41] and Bauge *et al.* [42])

and γ-ray strength function models for the $E1$ transition on the cross section of the reactions under study, considering fixed level density models. The calculations of the excitation functions proved to be insensitive with respect to the optical potential models. A dependency was revealed on the selection of the $E1$ γ-ray strength function models. This dependency, however, was only important when the constant temperature [34] and generalized superfluid [36,37] level density models were combined with some microscopic $E1$ γ-ray strength function models (models: 3, 4, and 8 of TALYS). In these cases the calculations showed larger discrepancies from the data at near threshold energies than the calculations based on the rest γ-ray strength function models.

The results for the isomeric state cross section adopting the phenomenological level density models are presented in Fig. 6(a). This figure shows that the generalized superfluid model [36,37] performs very well for the experimental data of the present study, as well as for the data reported by Luo [6], Fang [7], and Sakane [8]. A less satisfactory performance is noticed for the back-shifted Fermi gas model [35], especially
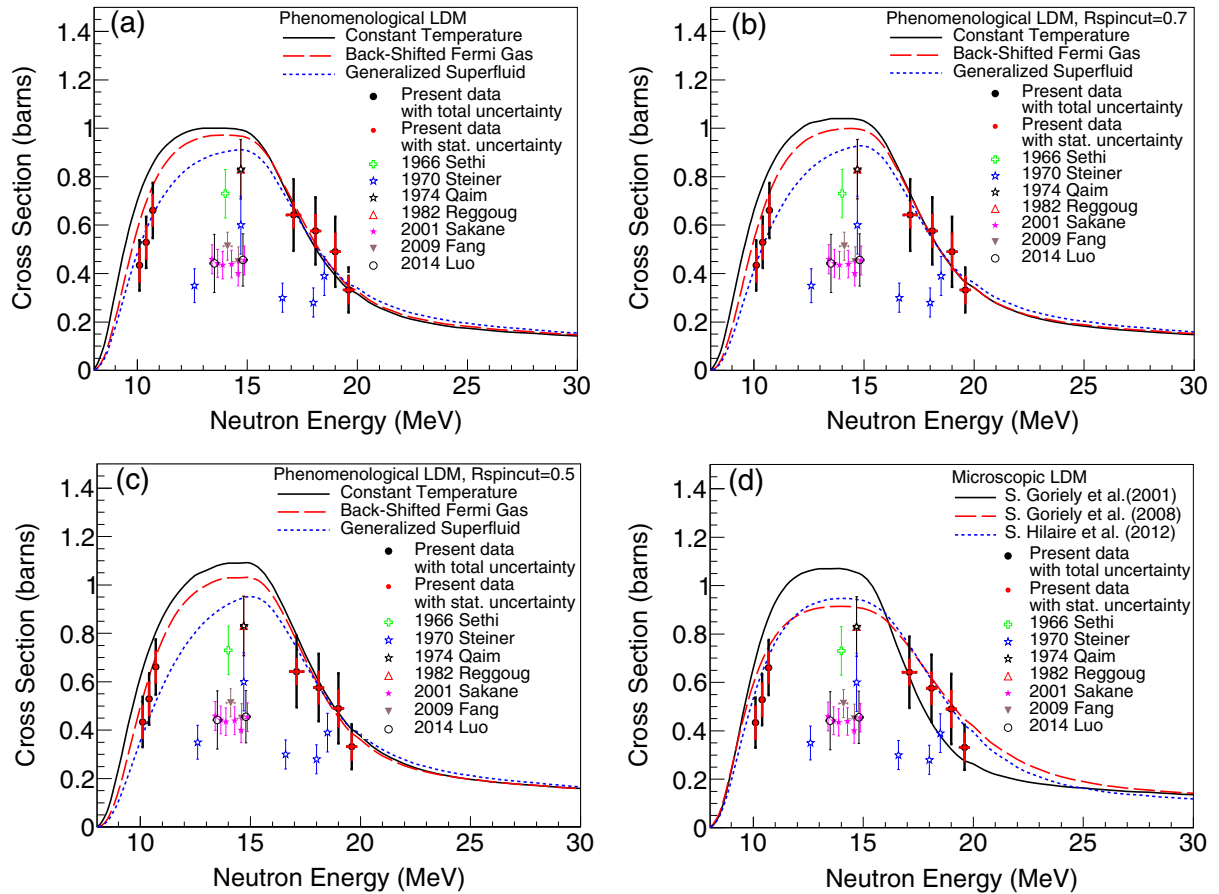
FIG. 7. The experimental data of the present and previous studies for the ^{165}Ho$(n, 2n)$ ^{164}Ho^g reaction along with the calculations based on the TALYS code (v. 1.9) for (a) the three phenomenological level density models: constant temperature model [34], back-shifted Fermi gas model [35], generalized superfluid model [36,37], (b) the three phenomenological level density models after setting "Rspincut" keyword equal to 0.7, (c) the three phenomenological level density models after setting "Rspincut" keyword equal to 0.5, and (d) the three microscopic level density models: Coriely *et al.* [38] (microscopic model 1), Goriely *et al.* [39] (microscopic model 2), and Hilaire *et al.* [40] (microscopic model 3). The experimental cross section data of the present work are presented with two different error bars corresponding to the statistical and total uncertainties.

at near threshold energies. At these energies, the most important discrepancies are noticed for the constant temperature model [34]. An important feature extracted from Fig. 6(a) is that all three phenomenological models are consistent for energies above 17 MeV.

In order to investigate the effect of the spin cut-off parameter in the feeding of the isomeric and ground state, the corresponding multiplicative parameter of TALYS, "Rspincut", was altered from the default value (=1) to 0.7 and 0.5. By reducing this parameter for the case of the isomeric state channel, as it is depicted in Figs. 6(b) and 6(c), the cross section decreases up to ≃18 MeV for all the phenomenological level density models. The generalized superfluid model [36,37] model still has a good agreement with the present data for both of the cases of "Rspincut" equal to 0.5 and 0.7. The behavior of the back-shifted Fermi gas model [35] is also improved, especially when "Rspincut" is reduced to 0.5. However, the agreement of the experimental points with the theoretical predictions at 10.4 and 10.7 MeV is at ≈2σ. The constant temperature model [34] still fails to reproduce the data at near threshold energies.

The TALYS calculations based on the microscopic level density models, demonstrated in Fig. 6(d), seem to present an inferior performance relevant to the data at near threshold energies. At energies above 17 MeV, only the microscopic model of Goriely *et al.* [38] (microscopic model 1) agrees with the reported in this work data.

Concerning the TALYS calculations of the excitation function for the population of the ground state, as previously, the generalized superfluid model [36,37] agrees with the present measurements. The theoretical predictions based on the back-shifted Fermi gas [35] and the constant temperature [34] models diverge from the data at near threshold energies. Between them the most important discrepancies are noticed for the constant temperature model [34]. Above 17 MeV all the phenomenological models follow the same trend, which is consistent with the data of this work [see Fig. 7(a)].

As can be seen from Figs. 7(b) and 7(c), when the "Rspincut" parameter is reduced, the cross section of the ground state decreases for energies up to ≃11 MeV and it increases for higher energies for the back-shifted Fermi gas [35] and the generalized superfluid [36,37] models. Concerning the
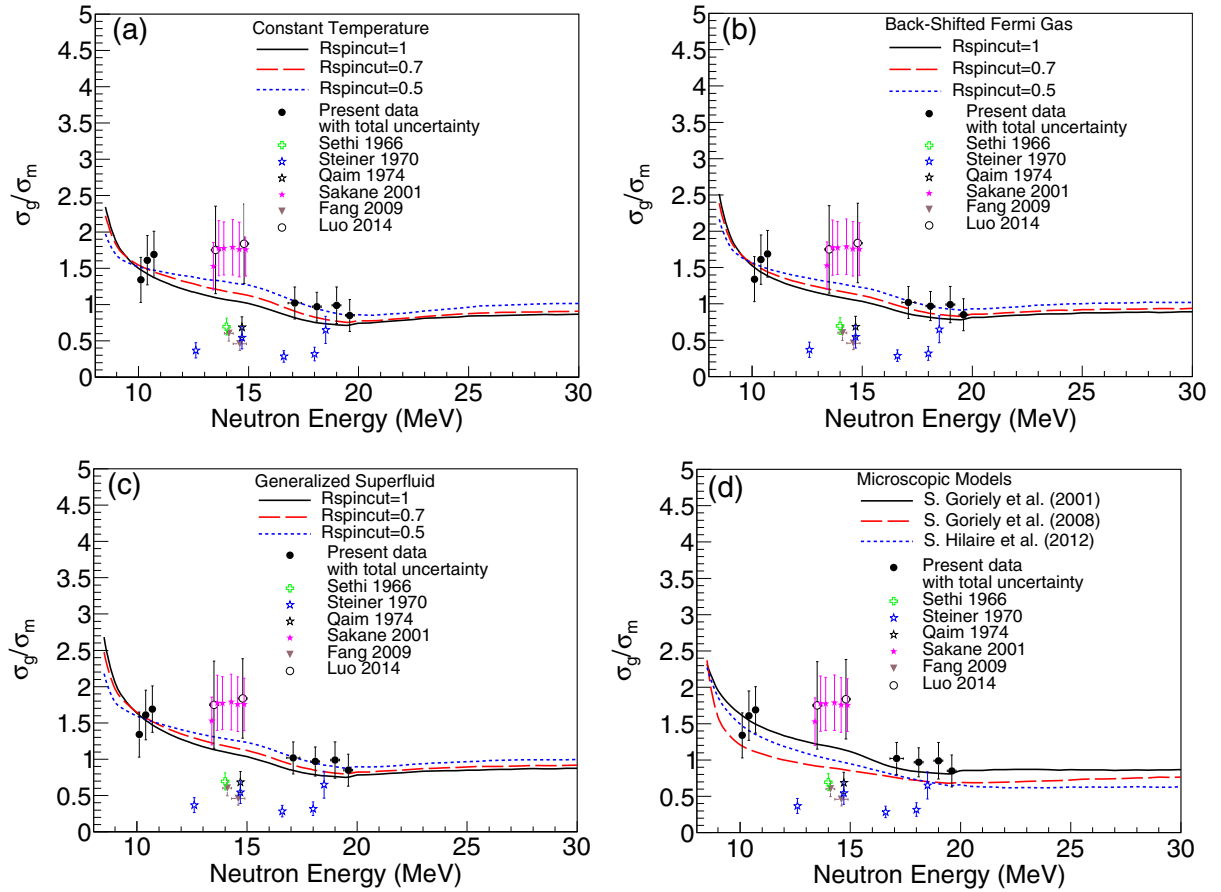
FIG. 8. The ratio of the cross section of the ^{165}Ho$(n, 2n)$ ^{164}Ho^g (σ_g) reaction to the cross section of the ^{165}Ho$(n, 2n)$ ^{164}Ho^m (σ_m) reaction for the experimental data of the present and previous studies along with the calculations based on the TALYS code (v. 1.9): (a) the constant temperature model [34] for different values of "Rspincut" keyword, (b) the back-shifted Fermi gas model [35] for different values of "Rspincut" keyword, (c) the generalized superfluid model [36,37] for different values of "Rspincut" keyword, and (d) the three microscopic level density models: Coriely *et al.* [38] (microscopic model 1), Goriely *et al.* [39] (microscopic model 2), and Hilaire *et al.* [40] (microscopic model 3).

constant temperature model [34], the cross section decreases up to $\simeq 13$ MeV and it increases for higher energies. Under this scope, the back-shifted Fermi gas [35] and the generalized superfluid models [36,37] are the ones which better follow the trend of the present data. After the reduction of "Rspincut" parameter, the constant temperature model still does not reproduce the data at near threshold energies. All models are still consistent in the high energy part of the excitation function, above 17 MeV.

Among the three microscopic level density models, the one of Hilaire *et al.* [40] (microscopic model 3) is closer to our data at near threshold energies, while all of them agree with the data for energies higher than 17 MeV [see Fig. 7(d)].

Concerning the cross sections ratio, as can be seen in Figs. 8(a)–8(d) the ratios resulting from the present work are compatible with the respective ratios resulting from all the TALYS calculations. Furthermore, Figs. 8(a)–8(c) show

TABLE V. The models and the parametrization of the TALYS code used in the calculations of the ^{165}Ho$(n, 2n)$ ^{164}Ho^m and ^{165}Ho$(n, 2n)$ ^{164}Ho^g reactions cross section.

optical model	level density model	$E1$ transition γ-ray strength function model	keyword: "fullhf"	keyword: "Rspincut"
Koning-Delaroche [41] or Bauge [42]	Constant temperature [34] Back-shifted Fermi gas [35] Generalized superfluid [36,37] microscopic model 1 [38] microscopic model 2 [39] microscopic model 3 [40]	Kopecky-Uhl [45]	yes	1, 0.7, 0.5

the impact of the spin cut-off parameter change on the cross sections ratio. In particular, for all the three phenomenological models, the decrease of the spin cut-off parameter leads to reduction of the ground to the isomeric state cross section ratio for energies up to $\simeq 10$ MeV, whereas for higher energies the corresponding ratio rises.

It should be noted that the TALYS level density models parametrization is defined by an optimization procedure, where the mean s-wave neutron level spacing at the neutron separation, $D0$, and the experimental discrete levels are taken into account following the process described in Ref. [47]. The change of the "Rspincut" keyword has an impact on the values of the spin cut-off parameter but the remaining parameters of the models, such as the energy dependent level density parameter α and the shell effects damping parameter γ, remain invariable. Therefore, through "Rspincut" keyword the level density is modified and not necessarily reproduces the observables. Applied modifications in "Rspincut", thus, aim at testing the sensitivity of the ground and isomeric state cross section to the spin distribution rather than suggesting an alternative model parametrization.

VII. SUMMARY AND CONCLUSIONS

In the present work the cross sections of the ^{165}Ho($n, 2n$)^{164}Ho^m and ^{165}Ho($n, 2n$)^{164}Ho^g reactions were studied for the first time at energies near the reaction threshold, namely at 10.1, 10.4, and 10.7 MeV, as well as in the high energy part at 17.1, 18.1, 19.0, and 19.6 MeV, following the activation technique relative to the ^{197}Au($n, 2n$)^{196}Au and ^{27}Al(n, α)^{24}Na reference reactions [18]. The neutron beams were produced via the ^{2}H(d, n)^{3}He (for neutron beam energies between 10–11 MeV) and ^{3}H(d, n)^{4}He (for neutron beam energies between 17–20 MeV) reactions. The irradiations were performed at the 5.5 MV Tandem Van de Graaff accelerator laboratory of the Institute of Nuclear and Particle Physics at N.C.S.R. "Demokritos".

The cross section of the isomeric state was deduced through the photopeak at 37.3 keV. Correction for x-ray escape peaks in this energy was applied using the GEANT4 code by reproducing the experimental spectra of the ^{164}Ho decay. To accurately measure the cross section of the ground state, its population from the isomeric state was taken into account during the irradiation time, the activity measurement time and their intermediate time, noted as "waiting time", given that the states have similar half-lives: $T_{1/2}^{m} = 36.6$ min and $T_{1/2}^{g} = 28.8$ min. The cross section of the ground state was calculated as the weighted average of the cross sections determined using the photopeaks at 73.4 and 91.4 keV.

The experimental data were compared with statistical calculations based on the TALYS code (v. 1.9). The performance of the code was investigated for the different inherent level density models. The adoption of different optical potentials for fixed level density models did not affect the excitation

functions of the reaction channels under study. The impact of different γ-ray strength functions for the $E1$ transition for fixed level density models was also searched. This impact was found strong only for the generalized superfluid [36,37] and the constant temperature [34] models, where the TALYS calculations of some γ-ray strength function microscopic models for the $E1$ transition (models: 3, 4, and 8 of TALYS) diverged more from the data at near threshold energies than the TALYS calculations corresponding to the rest models of the code. Taking into account all the calculations, it was concluded that the generalized superfluid model [36,37] is the one that performs better as far as the data of the present work are concerned for both the isomeric and the ground state and for the whole energy range, specially when the Kopecku-Uhl generalized Lorentzian model [45] is adopted for the $E1$ transition γ-ray strength functions.

The direct measurement of the feeding of the ground ($J^\pi = 1^+$) and the isomeric state ($J^\pi = 6^-$) allowed a sensitivity study with respect to the spin distribution of the formed compound nucleus, by reducing the value of the multiplicative factor of spin cut-off parameter, "Rspincut". However, even when "Rspincut" is reduced to 0.5 (default value=1), the back-shifted Fermi gas [35] and constant temperature [34] models do not reproduce the present data for both reaction channels over all energies. Therefore, it can be concluded that the excitation function of the ^{165}Ho($n, 2n$)^{164}Ho is not strongly dependent on the spin distribution. Concerning the microscopic approaches of the level densities, none of them reproduce the present data for both the isomeric and ground state over all energies.

In conclusion, through the present work, an improved mapping of the excitation functions of the ^{165}Ho($n, 2n$)^{164}Ho^m and ^{165}Ho($n, 2n$)^{164}Ho^g reactions was achieved from the reaction threshold up to 20 MeV, where the onset of the competitive ($n, 3n$) reaction channel occurs. These data along with the previous ones were used for the validation of the TALYS code (v. 1.9) theoretical estimations, considering the different level density models which are provided by the code.

[1] N. Patronis, C. T. Papadopoulos, S. Galanopoulos, M. Kokkoris, G. Perdikakis, R. Vlastou, A. Lagoyannis, and S. Harissopulos, Phys. Rev. C **75**, 034607 (2007).

[2] A. Kalamara, R. Vlastou, M. Kokkoris, N. G. Nicolis, N. Patronis, M. Serris, V. Michalopoulou, A. Stamatopoulos, A. Lagoyannis, and S. Harissopulos, Phys. Rev. C **97**, 034615 (2018).

[3] B. Singh and J. Chen, Nucl. Data Sheets **147**, 1 (2018).

[4] E. Georgali, Z. Eleme, N. Patronis, X. Aslanoglou, M. Axiotis, M. Diakaki, V. Foteinou, S. Harissopulos, A. Kalamara, M. Kokkoris, A. Lagoyannis, N. G Nicolis, G. Provatas, A. Stamatopoulos, S. Stoulos, A. Tsinganis, E. Vagena, R. Vlastou, and S. M. Vogiatzi, Phys. Rev. C **98**, 014622 (2018).

[5] K. S. Krane, *Introductory Nuclear Physics* (Wiley, New York, 1987).

[6] J. Luo and L. Jiang, Phys. Rev. C **89**, 014604 (2014).

[7] K. Fang, S. Xu, C. Lan, X. Xu, X. Kong, R. Liu, and L. Jiang, Appl. Radiation Isotopes **66**, 1104 (2008).

[8] H. Sakane, Y. Kasugai, M. Shibata, T. Iida, A. Takahashi, T. Fukahori, and K. Kawade, Ann. Nucl. Energy **28**, 1175 (2001).

[9] A. Reggoug, G. Paic, and M. Berrada, University of Mohammed V, Rabat, Annual Report No. 5, p. 14, 1982, https://www-nds.iaea.org/exfor/servlet/X4sGetSubent?reqx=113&subID=30698003.

[10] S. M. Qaim, Nucl. Phys. A **224**, 319 (1974).

[11] E. Steiner, P. Huber, W. Salathe, and R. Wagner, Helv. Phys. Acta **43**, 17 (1970).

[12] W. Dilg, H. Vonach, G. Winkler, and P. Hille, Nucl. Phys. A **118**, 9 (1968).

[13] M. Bormann, A. Behrend, I. Riehle, and O. Vogel, Nucl. Phys. A **115**, 309 (1968).

[14] H. O. Menlove, K. L. Coop, H. A. Grench, and R. Sher, Phys. Rev. **163**, 1308 (1967).

[15] B. Sethi and S. K. Mukherjee, Nucl. Phys. **85**, 227 (1966).

[16] K. Fang, Y. Xiang, Y. Han, X. Kong, T. Wang, R. Liu, and L. Jiang, Radiation Measurements **44**, 68 (2009).

[17] A. J. Koning, S. Hilaire, and M. C. Duijvestijn, TALYS -1.0, in *Proceedings of the International Conference on Nuclear Data for Science and Technology*, April 22–27, 2007, Nice, France, edited by O. Bersillon, F. Gunsing, E. Bauge, R. Jacqmin, and S. Leray (EDP Sciences, Les Ulis, France, 2008), pp. 211–214.

[18] International Reactor Dosimetry and Fusion File IRDFF v.1.05, 9 October 2014 https://www-nds.iaea.org/IRDFF/; R. Capote, K. I. Zolotarev, V. G. Pronyaev, and A. Trkov, J. ASTM Int. **9**, 104119 (2012); E. M. Zsolnay, R. Capote, H. K. Nolthenius, and A. Trkov, IAEA Technical Report No. INDC(NDS)-0616, 2012.

[19] E. Birgersson and G. Lovestam, JRC Science Hub Technical Report, Ref. No. 23794 (2009).

[20] J. F. Ziegler, J. P. Biersack, and M. D. Ziegler, SRIM-2008, available at http://www.srim.org/SRIM/SRIMLEGL.htm.

[21] GEANT4-A simulation toolkit, S. Agostinelli *et al.*, Nucl. Instrum. Methods. Phys. Res. A **506**, 250 (2003); IEEE Transactions Nuclear Science **53**, 270 (2006); Nucl. Instrum. Methods. Phys. Res. A **835**, 186 (2016).

[22] A. Kalamara, R. Vlastou, M. Kokkoris, M. Diakaki, A. Tsinganis, N. Patronis, M. Axiotis, and A. Lagoyannis, Phys. Rev. C **93**, 014610 (2016).

[23] A. Kalamara, N. Patronis, R. Vlastou, M. Kokkoris, S. Chasapoglou, A. Stamatopoulos, M. Serris, V. Paneta, M. Axiotis, A. Lagoyannis, S. Harissopulos, and I. E. Stamatelatos, Eur. Phys. J. A **55**, 187 (2019).

[24] Huang Xiaolong, Nucl. Data Sheets **108**, 1093 (2007).

[25] R. B. Firestone, Nucl. Data Sheets **108**, 2319 (2007).

[26] M. J. Martin, Nucl. Data Sheets **114**, 1497 (2013).

[27] B. Rosner and D. W. Mingay, Atomic Energy Board, Private Bag X256, Pretoria, South Africa.

[28] https://www-nds.iaea.org/exfor/exfor.htm.

[29] W. Hauser and H. Feshbach, Phys. Rev. **87**, 366 (1952).

[30] A. J. Koning and M. C. Duijvestijn, Nucl. Phys. A **744**, 15 (2004).

[31] H. Gruppelaar, P. Nagel, and P. E. Hodgson, Riv. Nuovo Cimento **9**, 1 (1986).

[32] E. Gadioli and P. E. Hodgson, *Pre-equilibrium Nuclear Reactions* (Oxford University Press, Oxford, 1992).

[33] T. Tamura, Rev. Mod. Phys. **37**, 679 (1965).

[34] A. Gilbert and A. G. W. Cameron, Can. J. Phys. **43**, 1446 (1965).

[35] W. Dilg, W. Schantl, H. Vonach, and M. Uhl, Nucl. Phys. A **217**, 269 (1973).

[36] A. V. Ignatyuk, K. K. Istekov, and G. N. Smirenkin, Yad. Fiz. **29**, 875 (1979) [Sov. J. Nucl. Phys. **29**, 450 (1979)].

[37] A. V. Ignatyuk, J. L. Weil, S. Raman, and S. Kahane, Phys. Rev. C **47**, 1504 (1993).

[38] S. Goriely, F. Tondeur, and J. M. Pearson, At. Data Nucl. Data Tables **77**, 311 (2001).

[39] S. Goriely, S. Hilaire, and A. J. Koning, Phys. Rev. C **78**, 064307 (2008).

[40] S. Hilaire, M. Girod, S. Goriely, and A. J. Koning, Phys. Rev. C **86**, 064317 (2012).

[41] A. J. Koning and J. P. Delaroche, Nucl. Phys. A **713**, 231 (2003).

[42] E. Bauge, J. P. Delaroche, and M. Girod, Phys. Rev. C **63**, 024607 (2001).

[43] D. M. Brink, Nucl. Phys. **4**, 215 (1957).

[44] P. Axel, Phys. Rev. **126**, 671 (1962).

[45] J. Kopecky and M. Uhl, Phys. Rev. C **41**, 1941 (1990).

[46] R. Capote, M. Herman, P. Oblozinsky, P. G. Young, S. Goriely, T. Belgya, A. V. Ignatyuk, A. J. Koning, S. Hilaire, V. Plujko, M. Avrigeanu, O. Bersillon, M. B. Chadwick, T. Fukahori, S. Kailas, J. Kopecky, V. M. Maslov, G. Reffo, M. Sin, E. Soukhovitskii, P. Talou, H. Yinlu, and G. Zhigang, Nucl. Data Sheets **110**, 3107 (2009).

[47] A. J. Koning *et al.*, Nucl. Phys. A **810**, 13 (2008).